THEMIS observations of electromagnetic ion cyclotron wave occurrence: Dependence on AE, SYMH, and solar wind dynamic pressure

M. E. Usanova,[1] I. R. Mann,[1] J. Bortnik,[2,3] L. Shao,[1] and V. Angelopoulos[4]

Received 19 June 2012; revised 29 August 2012; accepted 7 September 2012; published 12 October 2012.

[1] Electromagnetic ion cyclotron (EMIC) waves are transverse plasma waves generated by anisotropic proton distributions with $T_{perp} > T_{para}$. They are believed to play an important role in the dynamics of the ring current and potentially, of the radiation belts. Therefore it is important to know their localization in the magnetosphere and the magnetospheric and solar wind conditions which lead to their generation. Our earlier observations from three Time History of Events and Macroscale Interactions during Substorms (THEMIS) probes demonstrated that strong magnetospheric compressions associated with high solar wind dynamic pressure (P_{dyn}) may drive EMIC waves in the inner dayside magnetosphere, just inside the plasmapause. Previously, magnetospheric compressions were found to generate EMIC waves mainly close to the magnetopause. In this work we use an automated detection algorithm of EMIC Pc1 waves observed by THEMIS between May 2007 to December 2011 and present the occurrence rate of those waves as a function of L-shell, magnetic local time (MLT), P_{dyn}, AE, and SYMH. Consistent with earlier studies we find that the dayside (sunward of the terminator) outer magnetosphere is a preferential location for EMIC activity, with the occurrence rate in this region being strongly controlled by solar wind dynamic pressure. High EMIC occurrence, preferentially at 12–15 MLT, is also associated with high AE. Our analysis of 26 magnetic storms with Dst < −50 nT showed that the storm-time EMIC occurrence rate in the inner magnetosphere remains low (<10%). This brings into question the importance of EMIC waves in influencing energetic particle dynamics in the inner magnetosphere during disturbed geomagnetic conditions.

Citation: Usanova, M. E., I. R. Mann, J. Bortnik, L. Shao, and V. Angelopoulos (2012), THEMIS observations of electromagnetic ion cyclotron wave occurrence: Dependence on AE, SYMH, and solar wind dynamic pressure, *J. Geophys. Res.*, *117*, A10218, doi:10.1029/2012JA018049.

1. Introduction

[2] Electromagnetic ion cyclotron (EMIC) waves are predominately transverse left-hand polarized waves produced in the magnetosphere by anisotropic ($T_{perp} > T_{para}$) proton distributions in the Pc1–2 (0.1–5 Hz) frequency range. Early theoretical studies have shown that EMIC wave growth leads to isotropization of the initially unstable proton distribution and consequent pitch angle scattering and loss of particles into the ionosphere [e.g., *Cornwall*, 1965]. Ring current protons with energies of 10–100 keV are considered to be the source population that provides free energy for the EMIC instability. Theoretical studies have also shown that enhancement in cold plasma density is essential for EMIC wave amplification [*Cornwall et al.*, 1970; *Kozyra et al.*, 1984]. Therefore, for a long time the plasmapause region, where the hot and the cold ion populations overlap, was thought to be a preferential location for EMIC wave growth as well as for EMIC-related loss of ring current ions [e.g., *Cornwall et al.*, 1970] and potentially radiation belt electrons [e.g., *Bortnik et al.*, 2006]. Later, EMIC waves were found in plasmaspheric plumes – regions of enhanced cold plasma densities extending outward from the plasmasphere during magnetically disturbed times (see, e.g., case studies by *Fraser et al.* [2005], *Spasojević et al.* [2005], and *Morley et al.* [2009]).

[3] The effect of EMIC waves on ring current dynamics was also studied using kinetic simulations of ring current

[1]Department of Physics, University of Alberta Edmonton, Alberta Canada.
[2]Center for Solar-Terrestrial Research, New Jersey Institute of Technology, Newark, New Jersey, USA.
[3]Department of Atmospheric and Oceanic Sciences, University of California, Los Angeles, California, USA.
[4]Institute of Geophysics and Planetary Physics, University of California, Los Angeles, California, USA.

Corresponding author: M. E. Usanova, Department of Physics, University of Alberta, Edmonton, AB T6G 2E1, Canada. (musanova@ualberta.ca)

0148-0227/12/2012JA018049

evolution during geomagnetic storms [see, e.g., *Jordanova et al.*, 2006, and references therein]. Consistent with the case studies mentioned above, modeling demonstrated that EMIC wave activity maximizes during the storm main phase in the vicinity of the plasmapause or within the plasmaspheric plumes.

[4] Nevertheless, the relation between EMIC wave occurrence and enhanced plasma densities as well as their prevalence during the storm main phase still remains controversial. For example, statistical storm-time observations of EMIC waves at geosynchronous (GEO) orbit by *Fraser et al.* [2010] showed that only 29% of their events were observed during the storm main phase. A later study by *Halford et al.* [2010] using CRRES data found that during a more active decreasing solar cycle phase EMIC waves were found to occur 1.6 times more during storms than nonstorm times, though the probability of EMIC waves within the GEO orbit still had an average of only ~10% percent (A. Halford, personal communication, 2012). Also, a conjugate statistical survey of ground EMIC waves and geosynchronous cold plasma densities by *Posch et al.* [2010] revealed only a weak correspondence between EMIC wave occurrence and either plasmaspheric plumes or intervals of extended (to geosynchronous orbit) plasmapause. Their events were observed most often in association with increases in solar wind dynamic pressure.

[5] In situ EMIC wave occurrence was investigated earlier by *Anderson et al.* [1992] using magnetic field data from the AMPTE CCE satellite mission. AMPTE CCE event statistics was based on data from 1984 day 239 through 1985 day 326 and covered the range of L-shells between 3.5 and 9. These authors found that the EMIC occurrence distribution peaked at L > 7 in the early afternoon (12–15 MLT) and concluded that plasma sheet ions (on open drift paths) rather than ring current ions (on closed drift paths) provide the source for EMIC instability. In a subsequent study using AMPTE CCE data *Anderson and Hamilton* [1993] observed a strong correlation between EMIC waves in the 8–16 MLT, L > 6 region and sudden local magnetic field increases by 10–40%. They thus confirmed the earlier assumption by *Olson and Lee* [1983] that magnetospheric compressions enhance the keV proton temperature anisotropy and drive EMIC waves.

[6] Further, global in situ observations of EMIC waves between L = 3.5–8 were performed with data from the Combined Release and Radiation Effect Satellite (CRRES) which operated between 25 July 1990 and 11 October 1991 [*Fraser and Nguyen*, 2001]. On CRRES, EMIC waves were detected mainly between 14 and 16 MLT (with an additional small peak at 5 and 7 MLT) and at L = 6–7. Due to its lifetime, CRRES did not have a full MLT coverage, so events in the 9–11 MLT sector were absent. Also, the event occurrence was not normalized by the satellite dwell time; therefore, information about the occurrence rate is unavailable. An important aspect of the CRRES study was the analysis of EMIC wave location with respect to the plasmapause, which was identified from the gradient in electron density of >20 cm^{-3}/R_e. The analysis showed that EMIC waves were seen both inside and outside the plasmapause, therefore the plasmapause was not found to be a preferential location for EMIC wave generation.

[7] *Min et al.* [2012] analyzed the spectra of THEMIS magnetic field data between L = 3–12 from 1 April 2007 to 31 December 2010 and also considered EMIC wave spatial distributions. These authors did not distinguish between EMIC elements and broadband power enhancements in the EMIC band and were primarily concerned with wave spectral and propagation properties. They separated waves in the helium and hydrogen bands, and found that the helium band had peak occurrence in the dusk sector at L = 8–12 with hydrogen band occurrence peaking on the dawn sector at around L = 10–12. However, in agreement with the AMPTE CCE results, they also found highest occurrence on the highest L-shells and a very low EMIC occurrence at L < 8.

[8] The motivation for this study was the earlier observation of an EMIC wave event seen on THEMIS [*Usanova et al.*, 2008] where the waves were generated just inside the plasmapause during an interval of strong magnetospheric compression. In order to investigate how typical compression-related inner magnetosphere EMIC waves are, we used data from four THEMIS spacecraft (A, C, D, and E) between May 2007 to December 2011. In this work, we present observations of EMIC wave occurrence rates between L = 3–10 and focus on the response of EMIC wave occurrence to solar wind dynamic pressure, substorm (AE) and storm (SYMH) activity indices.

[9] This paper is organized as follows: First, we describe THEMIS orbits and instrumentation used for this study. Second, we present analysis of EMIC wave occurrence and compare our findings with earlier observations from AMPTE-CCE and CRRES satellites, reported by *Anderson et al.* [1992] and *Fraser and Nguyen* [2001], respectively. Then, we discuss the EMIC occurrence dependence on solar wind and geomagnetic indices. Discussion and conclusion end our paper.

2. THEMIS Orbits and Instrumentation

[10] The Time History of Events and Macroscale Interactions during Substorms (THEMIS) is a mission employing five identical microsatellites launched on February 17, 2007 [*Angelopoulos*, 2008]. The primary goal of THEMIS is to determine the large-scale evolution of substorm initiation in the magnetotail. However, the satellites also traverse the dayside magnetosphere, which allows for studying wave-particle interactions in the ring current and the radiation belts, in particular, processes leading to generation of EMIC waves. Right after launch, all spacecraft (A, B, C, D, and E) followed the same orbit with a 15.4 R_e apogee in a "string-of-pearls" configuration and in September 2007 were placed in highly elliptical orbits (THEMIS A apogee at 10 R_e, B at 30 R_e, C at 20 R_e, D and E at 12 R_e) where they lined up at apogee every 4 days. The line of apsides rotated once per 13 months 360° with respect to the Sun-Earth line, fully covering all MLT sectors of the magnetosphere. In December 2009, THEMIS B and C were sent to the Moon, while the remaining three probes continued orbiting the Earth with ~12 R_e apogee. Since THEMIS B had the highest apogee and spent most of its time outside the region of our interest, we excluded it from our analysis and hence used data only from THEMIS A, C, D, and E.

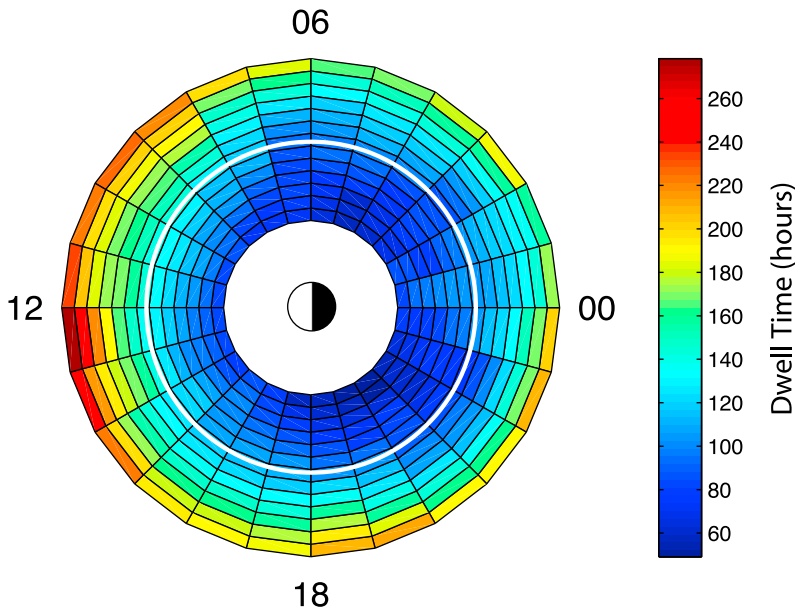

Figure 1. THEMIS A, C, D, and E combined dwell time in hours, plotted in L-MLT coordinates between L = 3–10. The white solid line shows the location of geosynchronous orbit (L = 6.6).

[11] For this work, we used magnetic field measurements from THEMIS FGM instruments [see *Auster et al.*, 2008] providing the most complete coverage in low resolution mode (FGL) at 4 samples/s (2 Hz Nyquist frequency) with accuracy of 0.01 nT. THEMIS dwell time in hours (except the intervals when FGM instruments were turned off) plotted in L-MLT coordinates between May 2007 and December 2011 is shown in Figure 1.

3. Automated Wave Detection Algorithm and Event Selection Criteria

[12] First, the magnetic field data has been transformed from the GSE into local field-aligned coordinates (FAC) following the method described in *Rae et al.* [2005]. In FAC, the azimuthal direction is perpendicular to both the direction of the background magnetic field and the radial direction, which lies in the plane containing the vector from the center of the Earth to the satellite. This allows us to analyze perpendicular (transverse) and parallel (compressional) magnetic field fluctuations independently. Further, we used the sliding window fast Fourier transform (FFT) to obtain a spectral power of the magnetic field. Finally, to identify EMIC Pc1 waves, we used an automated wave detection algorithm [*Bortnik et al.*, 2007], which selects spectral peaks that stand out (at least one magnitude greater in spectral power) above the background noise. This technique does not require a priori information about the wave spectrum such as the anticipated wave frequency and threshold spectral peak amplitude. Information on those properties is critical for the wave analysis used by *Anderson et al.* [1992] and *Min et al.* [2012].

[13] The EMIC wave instability can occur in three different frequency bands: below the oxygen, helium, and proton gyrofrequency. Technically, the oxygen mode can be observed in the Pc3 band (0.022–0.1 Hz) at high L-shells. However, since it may be confused with other wave activity typical to this band, e.g., dayside compressional waves originating from the shock region, we limited our analysis to the Pc1–2 (0.1–5 Hz) band only.

[14] In our case, we have chosen the window to be 1024 samples (256 s) long, with an overlap of ∼30% (80 s), resulting in ∼480 data blocks per day with a ∼180 s spacing between neighboring blocks. Since the background magnetic noise changes by orders of magnitude as the spacecraft pass through various magnetospheric regions, we also split the data into intervals with different background noise power. A spectral peak is detected when the averaged signal in a 3-min block exceeds the threshold noise level in the longer interval it belongs to. This results in three recorded frequencies: a bottom frequency, a top frequency, and a frequency of maximum power. An example of EMIC wave detection from the three THEMIS probes on 4 July 2007 is shown in Figure 2.

[15] The algorithm can identify multiband as well as single-band events. In this paper, we do not distinguish them and will focus on the spectral wave properties in our further study. If two spectral peaks occur simultaneously in two different frequency bands we treat them as a single event.

[16] Sometimes, the algorithm selects isolated peaks (also shown in Figure 2) that do not represent EMIC activity. To eliminate them from our further analysis, we added an additional criterion that there should be at least 4 consecutive peaks detected. In other words, the event should last at least 12 min.

[17] Following *Denton et al.* [2002], we identified magnetopause crossings (not shown here) from THEMIS

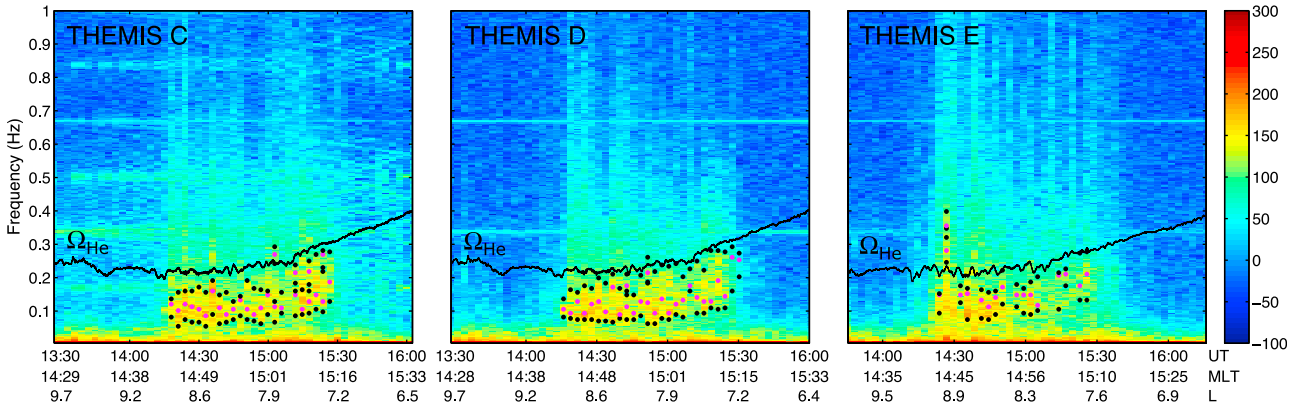

Figure 2. Example of EMIC wave identification on THEMIS C, D, and E from 4 July 2007. The wave activity was observed between ~14:20–14:30 MLT and L = 7.5–9. Superposed on each spectrogram is the local He gyrofrequency (black curve) and spectral peaks detected with the automated algorithm. The black and the purple dots define the bandwidth and the maximum power, respectively. See text for more details.

FGM spectrograms and also excluded the magnetosheath region characterized by broadband, large amplitude spectral fluctuations from our statistics.

4. Total EMIC Wave Occurrence Distribution

[18] Based on our selection criteria, we found ~26,000 EMIC spectral peaks (note that a single event may consist of ≥4 peaks) and a total of 1130 days between May 2007 and December 2011 with EMIC wave events. Further, knowing the position of each peak in the GSE coordinate system, we obtained its dipole L-value and MLT using the CXFORM coordinate transformation package (see http://nssdcftp.gsfc.nasa.gov/selected_software/coordinate_transform/). This allows us to plot the wave occurrence as a function of L and MLT. Of course, this does not take account of nondipole magnetic field distortions. However, since the THEMIS satellite orbits have low inclination, it provides reasonable and efficient estimate of the radial location of the waves mapped to the magnetic equatorial plane.

[19] We binned the peaks at 1 h resolution in MLT and 0.5 L in radial distance and normalized the EMIC wave distribution by THEMIS dwell time in each bin. The bin size was chosen large enough to be statistically significant for the event subsets presented in section 5, and containing at least forty 3 min intervals (minimum dwell time in each bin being 2 h). The resulting EMIC wave occurrence distribution in L-MLT coordinates is shown in Figure 3.

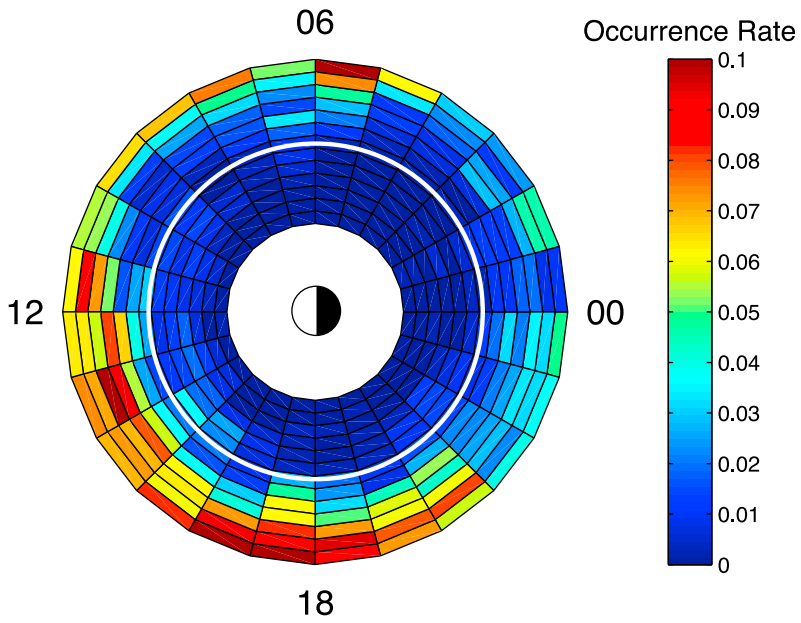

Figure 3. EMIC wave occurrence distribution, plotted in L-MLT coordinates between L = 3–10. The white solid line shows the location of geosynchronous orbit (L = 6.6) as above.

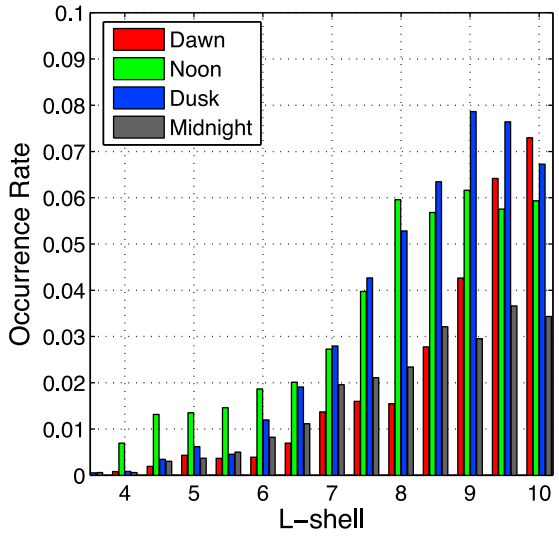

Figure 4. EMIC wave event occurrence as a function of L for the dawn, noon, dusk, and midnight sectors.

[20] Consistent with earlier AMPTE CCE [*Anderson et al.*, 1992] and CRRES [*Fraser and Nguyen*, 2001] studies, we found that the EMIC occurrence is higher in the dayside than in the nightside magnetosphere. Also, the waves are more likely to be observed at high L-shells, beyond geosynchronous orbit (white solid line overplotted on the histogram) with the probability reaching ~10%.

[21] The occurrence distribution for the dawn (3–9 MLT), noon (9–15 MLT), dusk (15–21 MLT), and midnight (21–3 MLT) sectors is shown in Figure 4. Generally, the occurrence rate increases with L in all four sectors. The MLT dependence of EMIC occurrence is consistent with the westward direction of the energetic ion drifts, assuming energetic ions provide the energy source for EMIC waves. The highest occurrence rate is observed in the noon and dusk sectors, reaching its maximum at L = 9. There is a finite but lower probability of detecting EMIC waves also in the dawn sector, where the maximum occurrence is observed at L = 10. The lowest occurrence rate of EMIC waves is on the midnight MLT sector.

[22] *Anderson et al.*, [1996] suggested that morning and afternoon EMIC waves have different ion source populations. Waves occurring from 10–18 MLT are generated by higher energy protons (>20 keV) that have drifted from the tail around the duskside. On the other hand, the morningside waves are driven by relatively fresh solar wind protons with lower energy (<5 keV) which followed drift paths past dawn directly from the tail and are not deflected westward toward dusk by their gradient curvature drifts.

[23] The histograms in Figure 4 also demonstrate that the inner magnetosphere event probability is higher in the noon sector than in the dusk, dawn, or midnight sectors, however it still does not exceed 2%. The occurrence distribution between L = 3.5–9 is generally consistent with results from the AMPTE CCE [*Anderson et al.*, 1992] mission, where L = 3.5–5 events had ≤1% probability, and L = 7–9 events occurred with 10–20% probability between 12 and 15 MLT and with 3% probability between 3 and 9 MLT. Also, similar to AMPTE CCE, we found a suppressed occurrence rate in the midnight sector. However, there are two main differences between the THEMIS and AMPTE CCE observations. First, our analysis shows that the region of enhanced occurrence rate extends further along the duskside, until 21 MLT. Second, the radial gap feature (a spatial separation between high-L and low-L events) seen in the morning sector by *Anderson et al.* [1992] is not present in the THEMIS statistics. On individual THEMIS passes, there does sometimes appear to be a gap between bursts of high-L and low-L EMIC waves but this is not borne out in the histograms.

5. EMIC Wave Occurrence Distribution for Different P_{dyn}, AE, and SYMH

[24] In this section, we investigate the relation between the EMIC wave occurrence and solar wind dynamic pressure, AE, Kp, and SYMH indices (accessed through the CDAWeb database, http://cdaweb.gsfc.nasa.gov). The solar wind dynamic pressure was obtained by combining the ACE and Wind satellite data time-shifted to the magnetopause [*King and Papitashvili*, 2004].

[25] The period between May 2007 and December 2011 is characterized by predominately quiet geomagnetic conditions. There are 23 moderate and 3 intense magnetic storms observed during this epoch (where the storm intervals are identified based on the Dst index falling below −50 nT), which are included in our statistics and also considered individually below. Figure 5 shows the total number of EMIC events (left panels) and their occurrence rate, i.e., total EMIC wave duration divided by spacecraft dwell time (right panels) as a function of solar wind dynamic pressure, P_{dyn} (red), AE (blue), SYMH (gray), and Kp*10 (green) indices. The EMIC occurrence rate increases with SYMH and Kp indices as well as with AE and P_{dyn}. Note that this is clearest for moderate values of AE and P_{dyn}, where the number of events in each bin remains high. We will consider these dependences in more detail in the sections below.

5.1. P_{dyn} Dependence

[26] Figure 6 shows EMIC occurrence distribution for four ranges of solar wind dynamic pressure: $0 < P_{dyn} < 1$, $0 < P_{dyn} < 1$, $1 < P_{dyn} < 2$, $2 < P_{dyn} < 3$, and $P_{dyn} > 3$ nPa. Since P_{dyn} rarely exceeded 4 nPa, and in order to provide good statistics for high dynamic pressure (as seen in Figure 5a), the last interval includes all the events with $P_{dyn} > 3$ nPa. As demonstrated in Figure 6, the EMIC occurrence rate increases significantly with solar wind dynamic pressure in the outer dayside magnetosphere (beyond the GEO orbit).

[27] Figure 7 also shows how the EMIC occurrence rate varies with P_{dyn} and L in the dawn, noon, dusk, and midnight sectors. The noon sector (green bars) is highly responsive to increases in solar wind dynamic pressure. The probability of EMIC occurrence increases with P_{dyn} mainly at high L-shells, close to the magnetopause, however, it also increases at lower L-shells as well, though less dramatically. Also, the maximum probability region moves inward with increased P_{dyn}, which may indicate magnetopause motion. The occurrence rate in the dawn sector (red bars) also grows with P_{dyn}, however, it maximizes at higher L-shells than in the noon sector, the difference being ~1 R_e. The EMIC probability in the dusk sector (blue bars) follows the noon sector for $1 < P_{dyn} < 2$, $2 < P_{dyn} < 3$ nPa, but exhibits a double-peak

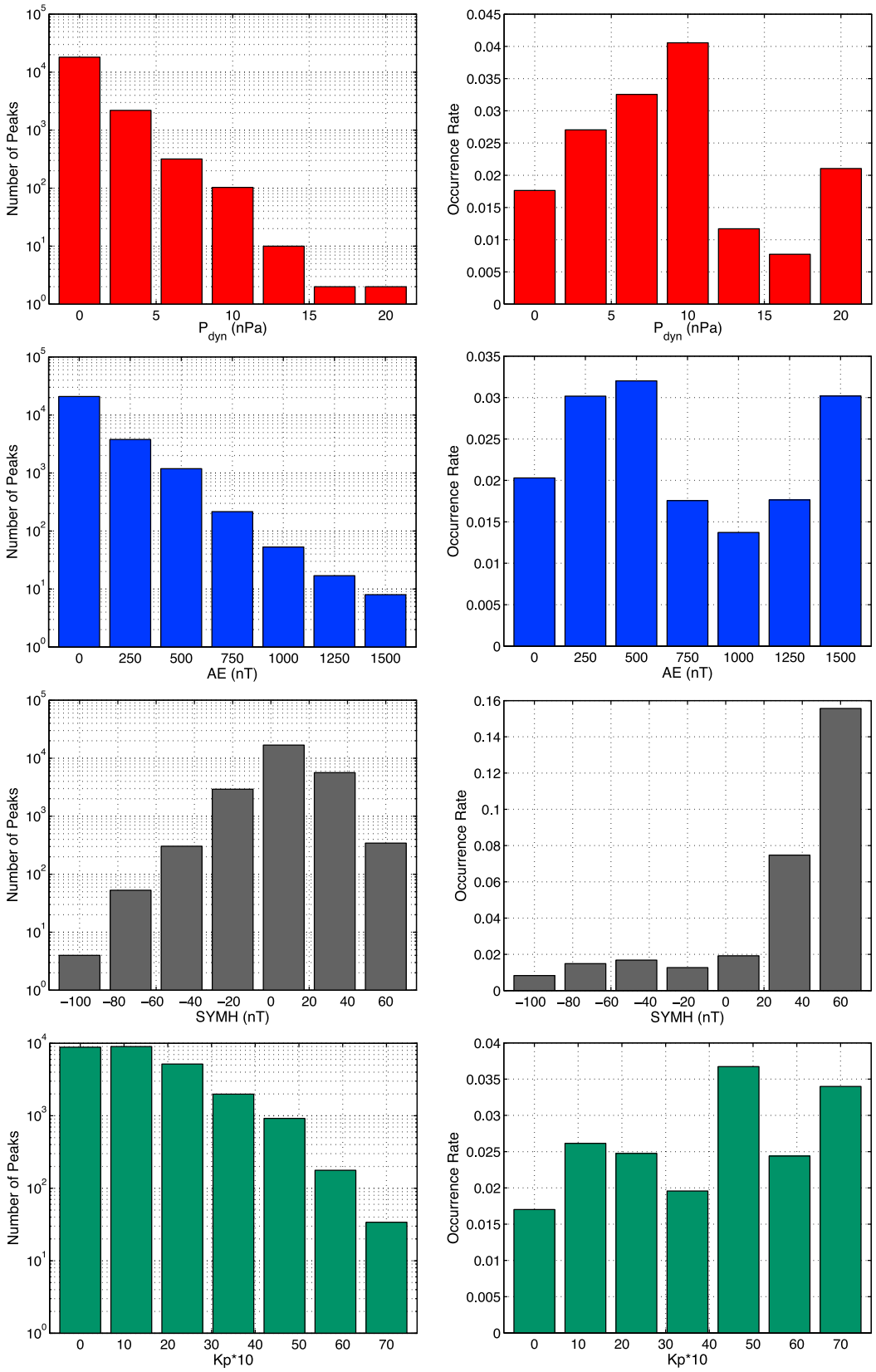

Figure 5. Number of (left) EMIC spectral peaks and (right) normalized occurrence, i.e., number of time windows with EMIC activity divided by number of time windows at specific activity range as a function of P_{dyn} (red), AE (blue), SYMH (gray), and Kp*10 (green). Note that panels of Figure 5 (left) are plotted on a logarithmic scale.

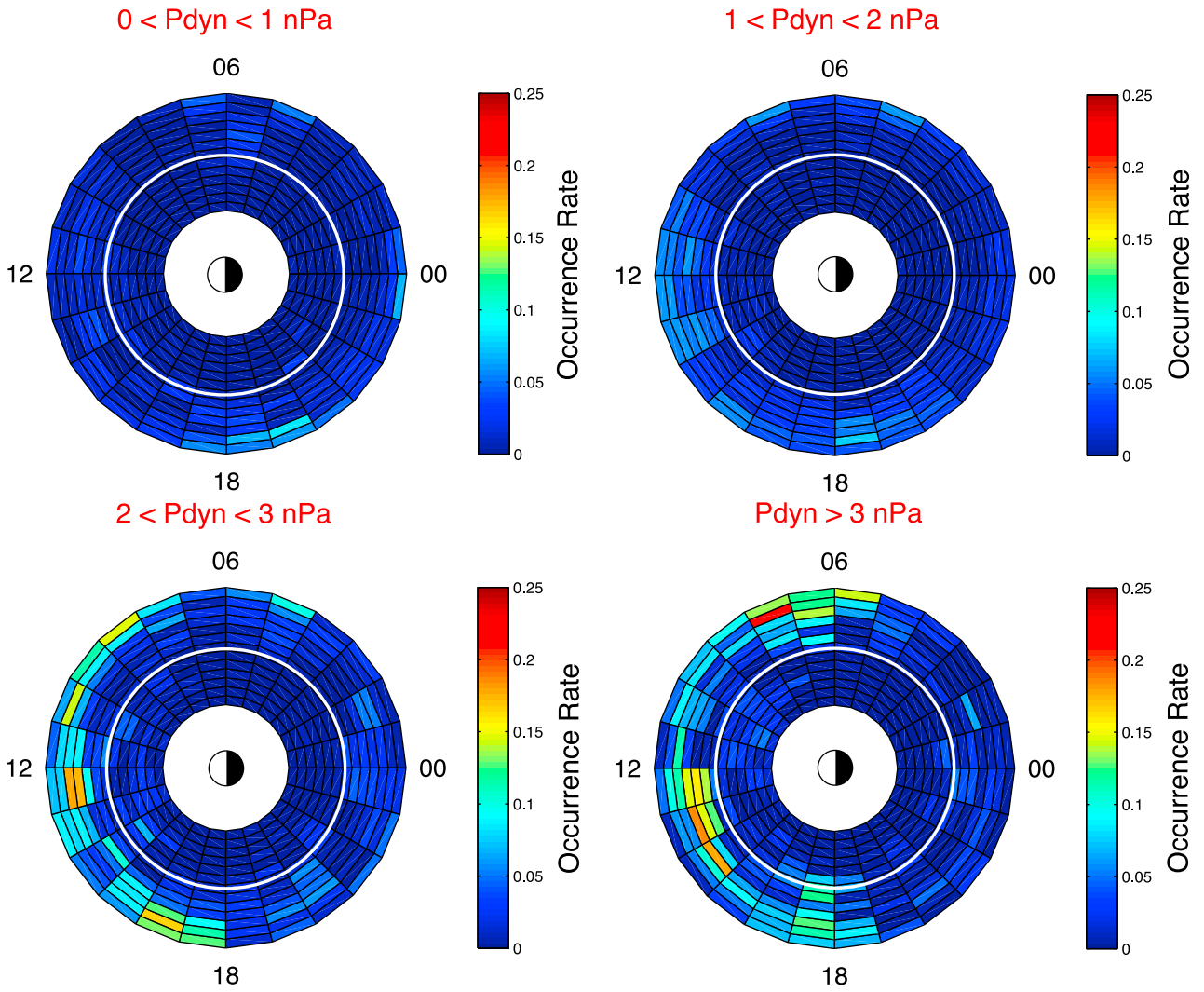

Figure 6. EMIC wave occurrence distribution (in L-MLT) for multiple intervals of solar wind dynamic pressure: $0 < P_{dyn} < 1$, $1 < P_{dyn} < 2$, $2 < P_{dyn} < 3$, and $P_{dyn} > 3$ nPa. The occurrence rate is color-coded from 0 (blue) to 0.25 (red). The white solid line in each panel shows the location of geosynchronous orbit (L = 6.6).

occurrence, at L = 6.5 and L = 8.5 for $P_{dyn} > 3$ nPa. Similar to the dawn/noon sector, the outer peak in the dusk sector maps close to the magnetopause; the second inner peak may be related to slightly enhanced wave growth in the expanded plasmasphere/plume region. However, future work is needed to examine this point further. The midnight sector (gray bars) does not seem to be significantly influenced by P_{dyn}.

5.2. AE Dependence

[28] In this section, we investigate the EMIC occurrence relation to the AE index, which serves as a proxy for substorm activity. We split the data into the intervals of low (AE < 100 nT), moderate (100 < AE < 300 nT) and enhanced (AE > 300 nT) activity. As shown in Figure 8, the EMIC occurrence rate increases with AE index. During intervals of moderate and enhanced substorm activity, the probability of observing EMIC waves is increased in the duskside magnetosphere, reaching ~10% in the postnoon-duskside sector.

[29] The overall distribution for four sectors is shown in Figure 9. For AE < 100 nT, the occurrence rate is minimal in the midnight sector (gray bars) and maximizes in the noon sector at L = 9 (green bars), and in the dawn sector at L = 9–10 (red bars). The probability increases for 100 < AE < 300 nT (see second panel in Figure 9) in the dusk and noon sectors beyond geosynchronous orbit, and maximizes at L = 9 in the noon and duskside sectors, and at L = 9.5 in the dawn sector. For AE > 300 nT the occurrence rate is maximal at L = 9 in the noon sector. Overall, the positive correlation between the probability of EMIC wave observation and AE is likely due to the injection and westward drift of energetic ion populations providing the energy source for EMIC waves. However, since intensifications in geomagnetic activity are often related to solar

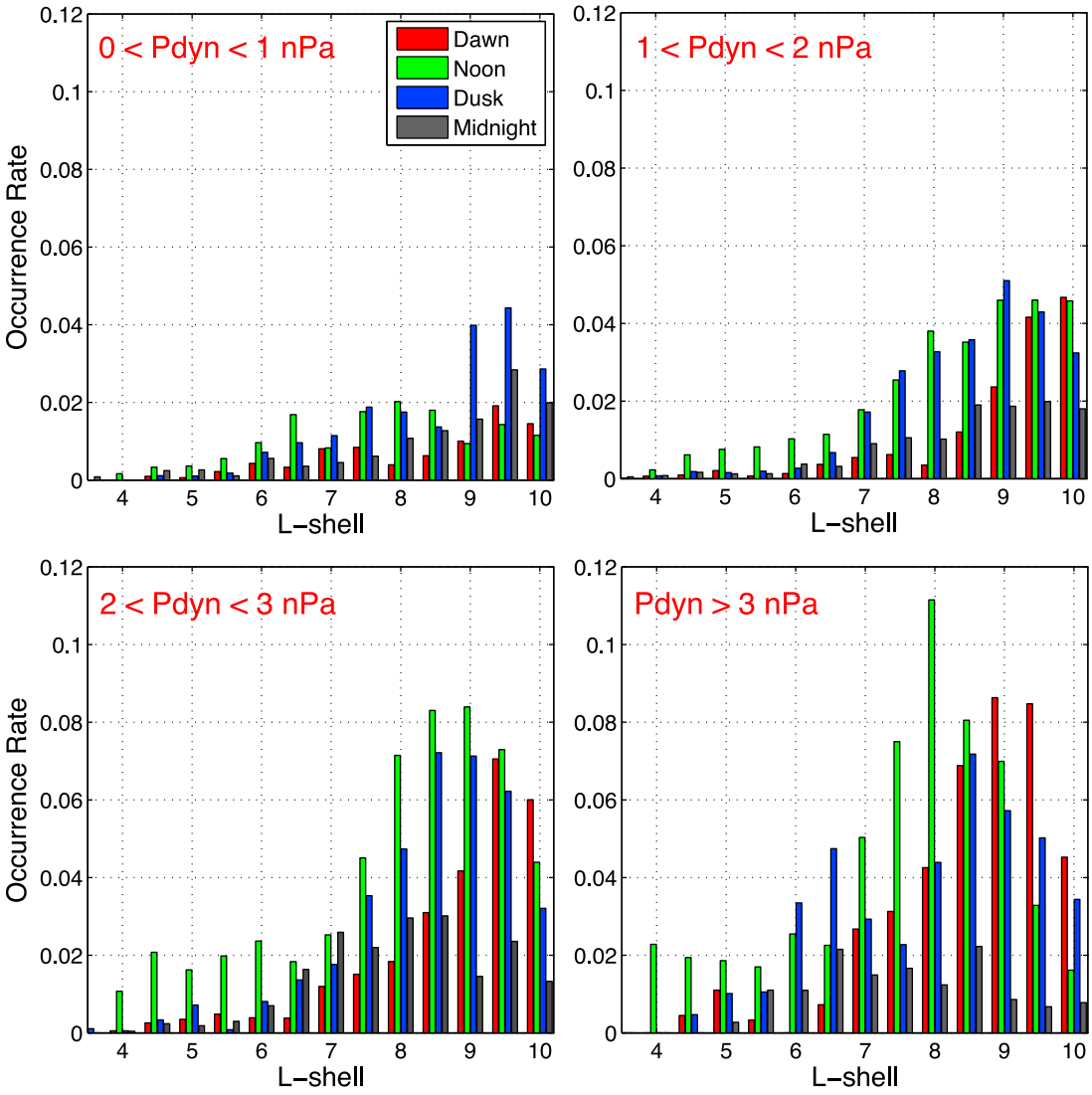

Figure 7. EMIC wave event occurrence as a function of L for the dawn (red), noon (green), dusk (blue), and midnight (black) sectors. The intervals of P_{dyn} are the same as in Figure 6.

wind pressure enhancements [see, e.g., *Tsurutani et al.*, 1985] it is unclear whether the EMIC wave activity was dominantly driven by internal, magnetospheric processes due to the disturbed geomagnetic conditions, by increased magnetopsheric compression, or by a combination thereof.

5.3. SYMH Dependence

[30] The hourly Dst index and its high-resolution (1 min) analog, the SYMH index are often used as a measure of magnetic storm activity. Storm main phase disturbances in SYMH are negative and are produced by the ring current. Positive disturbances are typically related to the current flowing along the magnetopause during magnetospheric compressions.

[31] The EMIC wave occurrence dependence on the SYMH index is shown in Figures 10 and 11. For SYMH < −20 nT, EMIC wave activity is observed mostly in the noon and duskside sectors and increases toward higher L-shells. EMIC wave occurrence in the inner magnetosphere remains around 2%, for SYMH < −20 nT, though the statistics of such events is low and further analysis for geomagnetically active periods is warranted. Our additional analysis of the main phase of the 26 magnetic storms with Dst < −50 nT (a subset of events with SYMH < −20 nT) showed that only 6 of them produced main-phase EMIC waves which were seen by the THEMIS A, C, D, or E satellites, both outside and inside the GEO orbit.

[32] For −20 < SYMH < −10 nT, the waves were detected mainly between 12 and 21 MLT with probability reaching 6% at high and <1% at low L-shells. For −10 nT < SYMH < 10 nT the occurrence rate (∼6%) is spread evenly in the outer dayside magnetosphere. Similar to the P_{dyn} dependence, the probability of EMIC wave observation increased significantly for SYMH > 10 nT. For SYMH > 10 nT, the region of maximum occurrence rate in the dayside moved inward to L = 8, and the probability increased in the inner dayside magnetosphere as well. The occurrence rate also increased significantly for the dawn

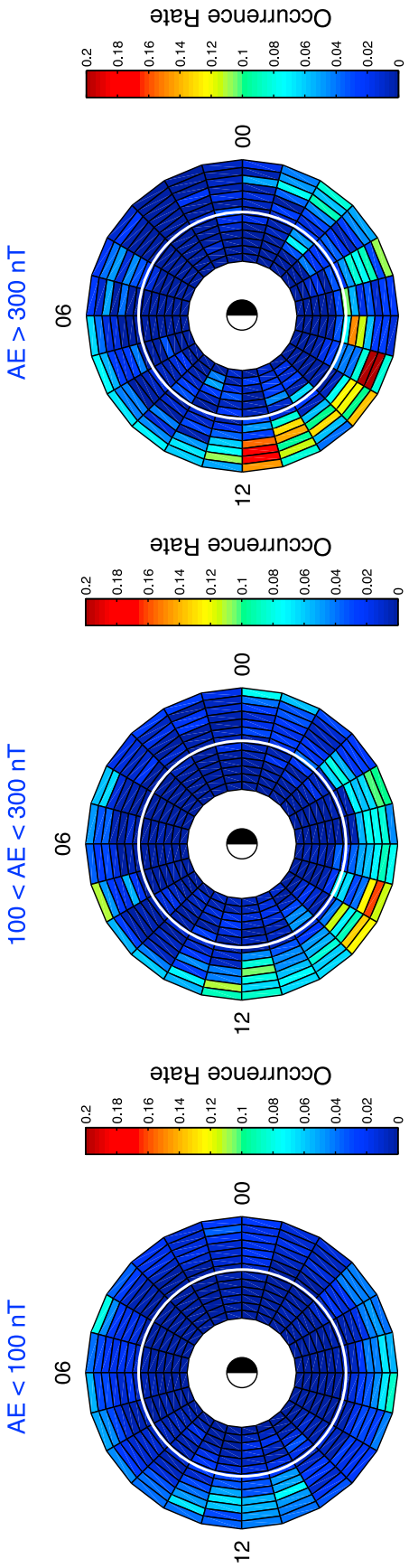

Figure 8. EMIC wave occurrence distribution (in L-MLT) for low (AE < 100 nT), moderate (100 < AE < 300 nT), and enhanced (AE > 300 nT) substorm activity. The occurrence rate is color-coded from 0 (blue) to 0.2 (red). The white solid line in each panel shows the location of geosynchronous orbit (L = 6.6).

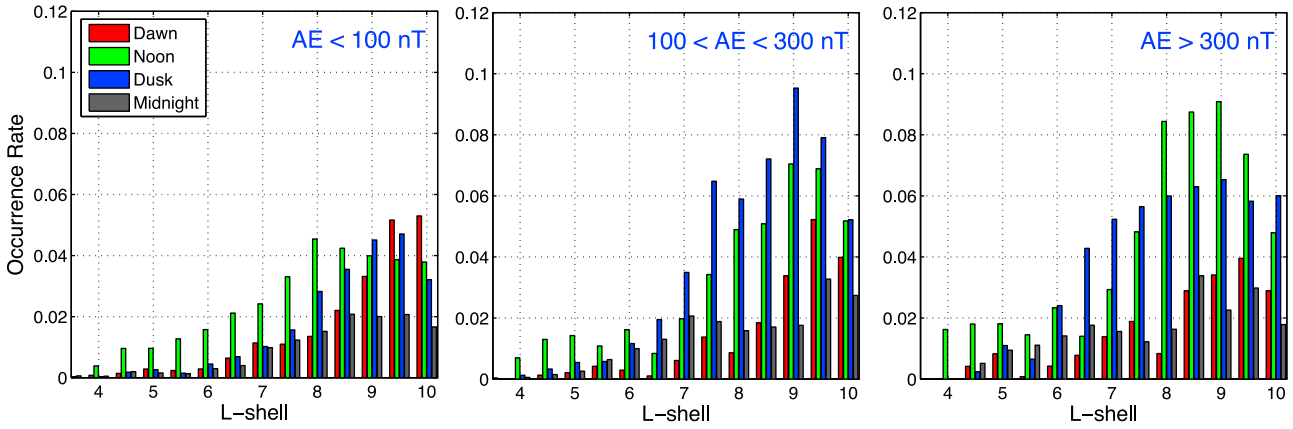

Figure 9. EMIC wave event occurrence as a function of L for the dawn (red), noon (green), dusk (blue), and midnight (black) sectors and three ranges of AE (AE < 100, 100 < AE < 300, and AE > 300 nT).

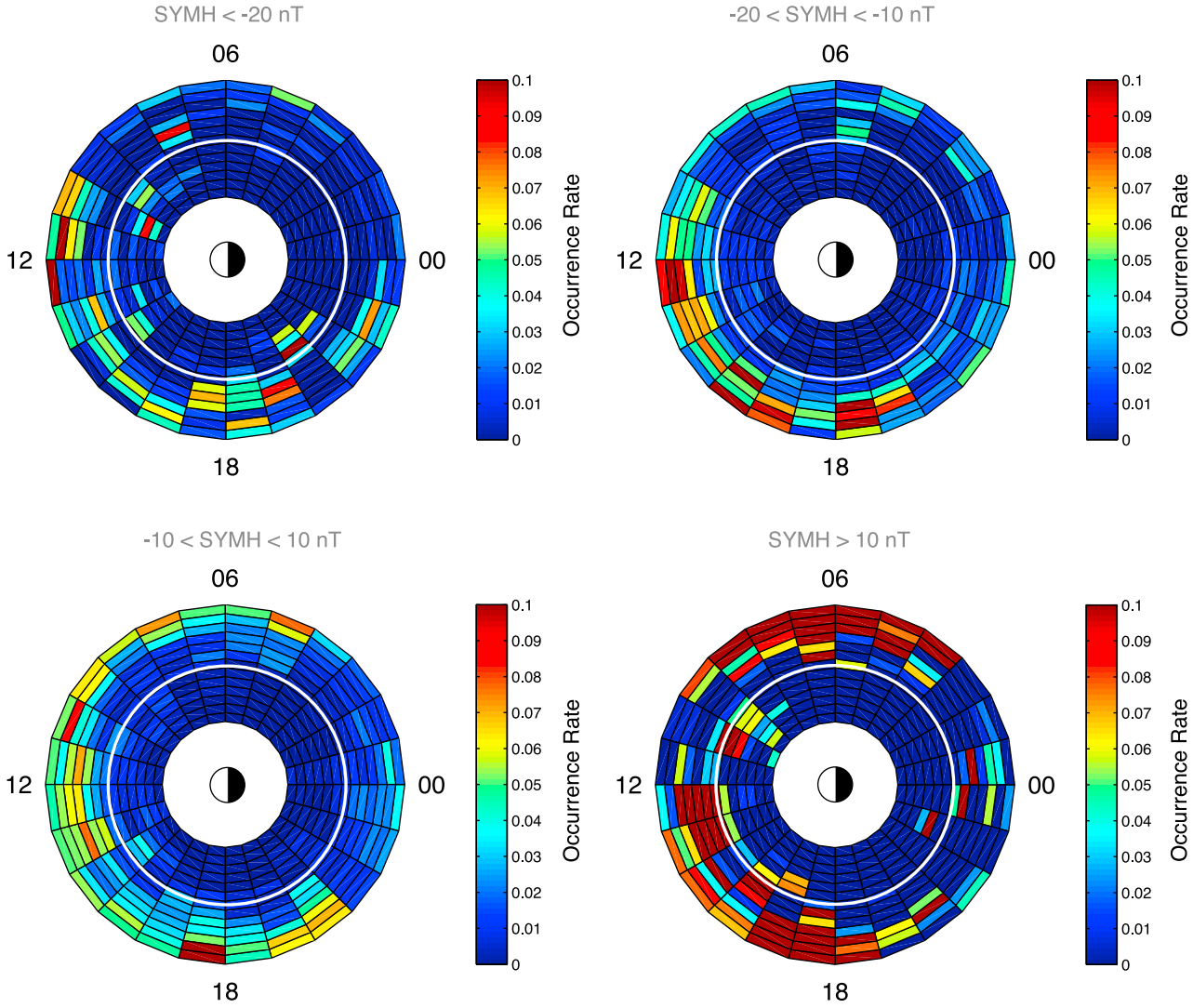

Figure 10. EMIC wave occurrence distribution (in L-MLT) for different intervals of SYMH (SYMH < −20, −20 < SYMH < −10, −10 < SYMH < 10, and SYMH > 10 nT). The white solid line in each panel shows geosynchronous orbit (L = 6.6).

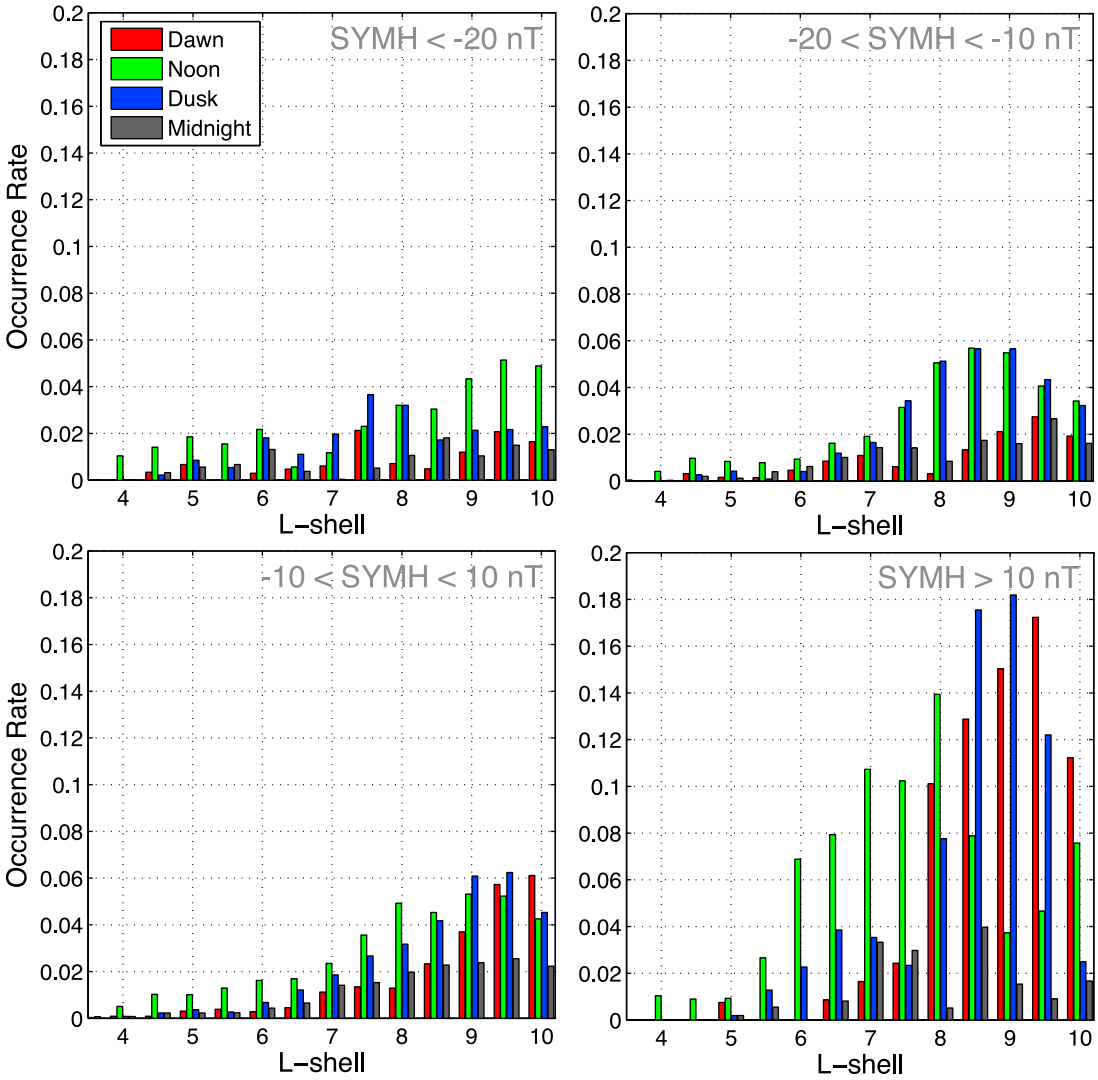

Figure 11. EMIC wave event occurrence as a function of L for the dawn (red), noon (green), dusk (blue), and midnight (black) sectors for different SYMH (SYMH < −20, −20 < SYMH < −10, −10 < SYMH < 10, and SYMH > 10 nT).

and dusk sectors with L-shell of maximum probability being L = 9.5 and L = 9 in each of these sectors, respectively.

6. Discussion on Physical Mechanisms for Compression-Related EMIC waves

[33] The prevalence of dayside EMIC activity during intervals of enhanced solar wind dynamic pressure can be explained by three possible mechanisms which can lead to the generation of anisotropic proton distributions. First, in the compressed magnetosphere ions exhibit so-called drift shell splitting: equatorially mirroring particles follow contours of constant magnetic field, while particles with smaller pitch angles drift around the Earth along more circular trajectories [see, e.g., *Sibeck et al.*, 1987]. When combined, they can form anisotropic distributions in the dayside magnetosphere (with $T_{perp} > T_{para}$), unstable to EMIC waves. Second, outer L-shells of the dayside magnetosphere have two off-equatorial magnetic field minima, also related to a compression-related reconfiguration of the magnetospheric magnetic field. Particles with 90° pitch angles drift through the equator but particles with lower pitch angles can mirror at high latitudes without passing through the equator, executing so-called Shabansky orbits. As a result, the ion perpendicular temperature near the equator increases relative to the parallel temperature, the resultant anisotropy giving rise to EMIC waves [see, e.g., *McCollough et al.*, 2012]. Both drift shell splitting and Shabansky mechanisms provide a continuous source of dayside anisotropy, lasting for several hours while the magnetosphere remains compressed. Third, short-term magnetospheric compressions can increase the T_{perp}/T_{para} ratio through adiabatic heating [see *Olson and Lee*, 1983] and can generate EMIC wave bursts during periods within which the magnetic field strength is increasing (i.e., $\frac{dB}{dt} > 0$).

7. Conclusions

[34] In this work, we analyzed THEMIS FGM data between May 2007 and December 2011. This is the largest data set ever used for statistical in situ EMIC wave analysis,

providing the most complete MLT coverage of the magnetosphere. For EMIC wave identification, we used the autodetection technique of *Bortnik et al.* [2007] that does not require a priori information about the wave spectrum (such as anticipated wave frequency and a threshold spectral peak amplitude). The technique also selects EMIC wave events that are bounded by power minima at higher and lower frequencies in the dynamic spectra.

[35] Our analysis showed that quiet time EMIC activity is typically a dayside outer magnetosphere phenomenon, and that the EMIC occurrence rate increases toward the magnetopause, which is consistent with earlier observations by *Anderson et al.* [1992], *Fraser and Nguyen* [2001], and *Denton et al.* [2002].

[36] We investigated the EMIC occurrence rate in relation to solar wind dynamic pressure, AE, and SYMH indices and found that P_{dyn} is a major factor affecting the occurrence of EMIC waves during quiet geomagnetic conditions. We found a ~15% probability of observing dayside EMIC waves beyond geosynchronous orbit during increased P_{dyn} or positive SYMH (both signatures of magnetospheric compression).

[37] The EMIC occurrence rate in the inner magnetosphere (below the GEO orbit) is around only a few percent. We found increased EMIC wave occurrence inside the GEO orbit in the duskside sector during $P_{dyn} > 3$ nPa, though the probability still does not exceed ~5%. On several cases high solar wind dynamic pressure drives EMIC waves inside the GEO orbit in the noon sector (in line with our earlier studies [e.g., *Usanova et al.*, 2008, 2010]). However, since extreme enhancements in solar wind dynamic pressure are relatively infrequent, we could not examine this statistically with the data available here.

[38] From our EMIC wave survey, we also investigated wave occurrence during the main storm phase. Analysis of 26 magnetic storms with Dst < 50 nT showed that EMIC probability during the storm main phase is ~20% (seen in only 6 out of 26 storms). For these storm events, EMIC waves were observed both outside and inside of geosynchronous orbit.

[39] Overall, our analysis demonstrated that the occurrence rate of EMIC waves in the inner magnetosphere is low, both during quiet and disturbed geomagnetic conditions. Therefore, the importance of EMIC waves for influencing the dynamics of energetic particles in the ring current and radiation belts must be carefully assessed.

[40] **Acknowledgments.** Thanks to K. H. Glassmeier, U. Auster and W. Baumjohann for the use of FGM data provided under the lead of the Technical University of Braunschweig and with financial support through the German Ministry for Economy and Technology and the German Center for Aviation and Space (DLR) under contract 50 OC 0302, Ed Santiago and Ryan Boller for the coordinate transformation routine, and CDAWeb for OMNI solar wind parameters and geomagnetic indices. This work is supported in part by participation in the Monitoring, Analyzing and Assessing Radiation Belt Loss and Energization (MAARBLE) consortium. MAARBLE has received funding from the European Community's Seventh Framework Programme (FP7-SPACE-2010-1, SP1 Cooperation, Collaborative project) under grant agreement number 284520. This paper reflects only the authors' views and the Union is not liable for any use that may be made of the information contained herein. IRM is supported by a Discovery Grant from Canadian NSERC. MEU is partly supported by the Canadian Space Agency. THEMIS is funded by NASA contract NAS5–02099.

[41] Robert Lysak thanks the reviewers for their assistance in evaluating this paper.

References

Anderson, B. J., and D. J. Hamilton (1993), Electromagnetic ion cyclotron waves stimulated by modest magnetospheric compressions, *J. Geophys. Res.*, *98*, 11,369–11,382, doi:10.1029/93JA00605.

Anderson, B. J., R. E. Erlandson, and L. J. Zanetti (1992), A statistical study of Pc 1–2 magnetic pulsations in the equatorial magnetosphere, 1. Equatorial occurrence distributions, *J. Geophys. Res.*, *97*(A3), 3075–3088, doi:10.1029/91JA02706.

Anderson, B. J., R. E. Denton, G. Ho, D. C. Hamilton, S. A. Fuselier, and R. J. Strangeway (1996), Observational test of local proton cyclotron instability in the Earth's magnetosphere, *J. Geophys. Res.*, *101*(A10), 21,527–21,543, doi:10.1029/96JA01251.

Angelopoulos, V. (2008), The THEMIS mission, *Space Sci. Rev.*, *141*, 5–34, doi:10.1007/s11214-008-9336-1.

Auster, H. U., et al. (2008), The THEMIS fluxgate magnetometer, *Space Sci. Rev.*, *141*, 235–264, doi:10.1007/s11214-008-9365-9.

Bortnik, J., R. M. Thorne, T. P. O'Brien, J. C. Green, R. J. Strangeway, Y. Y. Shprits, and D. N. Baker (2006), Observation of two distinct, rapid loss mechanisms during the 20 November 2003 radiation belt dropout event, *J. Geophys. Res.*, *111*, A12216, doi:10.1029/2006JA011802.

Bortnik, J., J. W. Cutler, C. Dunson, and T. E. Bleier (2007), An automatic wave detection algorithm applied to Pc1 pulsations, *J. Geophys. Res.*, *112*, A04204, doi:10.1029/2006JA011900.

Cornwall, J. M. (1965), Cyclotron instabilities and electromagnetic emissions in the ultra low frequency and very low frequency ranges, *J. Geophys. Res.*, *70*, 61–69, doi:10.1029/JZ070i001p00061.

Cornwall, J. M., F. V. Coroniti, and R. M. Thorne (1970), Turbulent loss of ring current protons, *J. Geophys. Res.*, *75*(25), 4699–4709, doi:10.1029/JA075i025p04699.

Denton, R. E., J. LaBelle, and X. Zhu (2002), Location of Pc 1–2 waves relative to the magnetopause, *Ann. Geophys.*, *20*, 1763–1767, doi:10.5194/angeo-20-1763-2002.

Fraser, B. J., and T. S. Nguyen (2001), Is the plasmapause preferred source region of electromagnetic ion cyclotron waves in the magnetosphere?, *J. Atmos. Sol. Terr. Phys.*, *63*, 1225–1247, doi:10.1016/S1364-6826(00)00225-X.

Fraser, B. J., H. J. Singer, M. L. Adrian, D. L. Gallagher, and M. F. Thomsen (2005), The relationship between plasma density structure and EMIC waves at geosynchronous orbit, in *Inner Magnetosphere Interactions: New Perspectives From Imaging*, *Geophys. Monogr. Ser*, vol. 159, edited by J. Burch, M. Schulz, and H. Spence, pp. 55–70, AGU, Washington, D. C., doi:10.1029/159GM04.

Fraser, B. J., R. S. Grew, S. K. Morley, J. C. Green, H. J. Singer, T. M. Loto'aniu, and M. F. Thomsen (2010), Storm time observations of electromagnetic ion cyclotron waves at geosynchronous orbit: GOES results, *J. Geophys. Res.*, *115*, A05208, doi:10.1029/2009JA014516.

Halford, A. J., B. J. Fraser, and S. K. Morley (2010), EMIC wave activity during geomagnetic storm and nonstorm periods: CRRES results, *J. Geophys. Res.*, *115*, A12248, doi:10.1029/2010JA015716.

Jordanova, V. K., Y. S. Miyoshi, S. Zaharia, M. F. Thomsen, G. D. Reeves, D. S. Evans, C. G. Mouikis, and J. F. Fennell (2006), Kinetic simulations of ring current evolution during the Geospace Environment Modeling challenge events, *J. Geophys. Res.*, *111*, A11S10, doi:10.1029/2006JA011644.

King, J. H., and N. E. Papitashvili (2004), Solar wind spatial scales in and comparisons of hourly Wind and ACE plasma and magnetic field data, *J. Geophys. Res.*, *110*, A02209, doi:10.1029/2004JA010804.

Kozyra, J. U., T. E. Cravens, F. Nagy, and E. G. Fontheim (1984), Effects of energetic heavy ions on electromagnetic ion cyclotron wave generation in the plasmapause region, *J. Geophys. Res.*, *89*(A4), 2217–2233, doi:10.1029/JA089iA04p02217.

McCollough, J. P., S. R. Elkington, and D. N. Baker (2012), The role of Shabansky orbits in compression-related electromagnetic ion cyclotron wave growth, *J. Geophys. Res.*, *117*, A01208, doi:10.1029/2011JA016948.

Min, K., J. Lee, K. Keika, and W. Li (2012), Global distribution of EMIC waves derived from THEMIS observations, *J. Geophys. Res.*, *117*, A05219, doi:10.1029/2012JA017515.

Morley, S. K., S. T. Ables, M. D. Sciffer, and B. J. Fraser (2009), Multipoint observations of Pc1–2 waves in the afternoon sector, *J. Geophys. Res.*, *114*, A09205, doi:10.1029/2009JA014162.

Olson, J. V., and L. C. Lee (1983), Pc1 wave generation by sudden impulses, *Planet. Space Sci.*, *31*, 295–302, doi:10.1016/0032-0633(83)90079-X.

Posch, J. L., M. J. Engebretson, M. T. Murphy, M. H. Denton, M. R. Lessard, and R. B. Horne (2010), Probing the relationship between electromagnetic ion cyclotron waves and plasmaspheric plumes near geosynchronous orbit, *J. Geophys. Res.*, *115*, A11205, doi:10.1029/2010JA015446.

Rae, I. J., et al. (2005), Evolution and characteristics of global Pc5 ULF waves during a high solar wind speed interval, *J. Geophys. Res.*, *110*, A12211, doi:10.1029/2005JA011007.

Sibeck, D. G., R. W. McEntire, A. T. Y. Lui, R. E. Lopez, and S. M. Krimigis (1987), Magnetic field drift shell splitting—Cause of unusual dayside particle pitch angle distributions during storms and substorms, *J. Geophys. Res.*, *92*, 13,485–13,497, doi:10.1029/JA092iA12p13485.

Spasojević, M., M. R. Thomsen, P. J. Chi, and B. R. Sandel (2005), Afternoon subauroral proton precipitation resulting from ring current—Plasmasphere interaction, in *Inner Magnetosphere Interactions: New Perspectives From Imaging*, *Geophys. Monogr. Ser*, vol. 159, edited by J. Burch, M. Schulz, and H. Spence, pp. 85–99, AGU, Washington, D. C., doi:10.1029/159GM06.

Tsurutani, B. T., J. A. Slavin, Y. Kamide, R. D. Zwickl, J. H. King, and C. T. Russell (1985), Coupling between the solar wind and the magnetosphere: CDAW 6, *J. Geophys. Res.*, *90*(A2), 1191–1199, doi:10.1029/JA090iA02p01191.

Usanova, M. E., I. R. Mann, I. J. Rae, Z. C. Kale, V. Angelopoulos, J. W. Bonnell, K.-H. Glassmeier, H. U. Auster, and H. J. Singer (2008), Multipoint observations of magnetospheric compression-related EMIC Pc1 waves by THEMIS and CARISMA, *Geophys. Res. Lett.*, *35*, L17S25, doi:10.1029/2008GL034458.

Usanova, M. E., et al. (2010), Conjugate ground and multisatellite observations of compression-related EMIC Pc1 waves and associated proton precipitation, *J. Geophys. Res.*, *115*, A07208, doi:10.1029/2009JA014935.